Journal of Fluorine Chemistry 206 (2018) 48–53

Contents lists available at ScienceDirect

Journal of Fluorine Chemistry

journal homepage: www.elsevier.com/locate/fluor

Solvent effect on 3D topology of hybrid fluorides: Synthesis, structure and luminescent properties of Zn(II) coordination compounds

Vanessa Pimenta[a], Marine Oger[a], Guillaume Salek[b], Annie Hemon-Ribaud[a], Marc Leblanc[a], Gilles Dujardin[a], Vincent Maisonneuve[a,*], Jérôme Lhoste[a]

[a] LUNAM Université, Université du Maine, CNRS UMR 6283, Institut des Molécules et Matériaux du Mans (IMMM), Avenue Olivier Messiaen, 72085 Le Mans Cedex 9, France

[b] Institut de Chimie de la Matière Condensée de Bordeaux (ICMCB), Université de Bordeaux, CNRS UPR 9048, 87 Avenue du Dr Albert Schweitzer, Pessac 33608 Cedex, France

ARTICLE INFO

Keywords:
Hybrid fluoride
Tetrazole
MOF
Solvothermal synthesis
Microwave heating

ABSTRACT

The mixture $ZnF_2/HF_{aq.}/H$*amtetraz* (H*amtetraz* = 5-aminotetrazole) with the molar ratio 10/80/10 reacts at 160 °C in different solvents (methanol/water and water respectively) to give two new 3D compounds: $(Zn_4F_4(amtetraz)_4)\cdot H_2O$ (1) and $(Zn_4F_4(H_2O)(amtetraz)_4)\cdot H_2O$ (2). The structures, determined by single crystal X-ray diffraction, exhibit neutral 3D-frameworks with narrow cavities that contain water molecules. Each network is built up from two types of parallel chains connected by aminotetrazolate ligands. The comparison of 1 and 2 with literature compounds shows that the nature of the polar solvent, aprotic or protic, influences the network characteristics, as well as the condensation of inorganic species or the bridging mode of the organic moieties. The luminescence properties of the zinc fluoro-aminotetrazolates are discussed.

1. Introduction

Porous coordination compounds, also known as Metal-Organic Frameworks (MOFs), have emerged during the last two decades. These hybrid compounds are nowadays considered as a new generation of multifunctional materials for potential applications in several fields, such as gas storage, health, catalysis or luminescent devices [1–4]. The desired properties can be tuned by combining the inorganic units, commonly built up from 3*d* metals or lanthanides [5–8] and the organic linkers, mainly carboxylic acids or azoles [9,10]. Azole ligands are extremely versatile linkers due to their heterocyclic character, in particular tetrazole derivatives [11]. Four nitrogen atoms, available in tetrazole rings, allow a broad range of bridging modes, opening the way to the design of new porous crystalline buildings with a remarkable structural diversity [10].

Whether the nature of the organic and inorganic entities plays a key role [12–15], it has been demonstrated that reaction conditions such as the synthesis temperature, the solvent or the pH [16–18] can strongly influence on framework design. Although very numerous examples of MOFs based on carboxylic acid linkers are available [19,20], fewer studies are reported for azole based networks [21,22], and those on fluorinated being downright scarce [23].

Our recent work has been focused on the deep understanding of the influence of the synthesis parameters in azole based fluorinated networks, for instance, the molar ratio between the starting reactants and the synthesis temperature. We have shown that for fluorine rich compositions, hybrids with covalent bonds between the organic and inorganic entities and with high dimensionalities are favoured [24,25]. Moreover we have demonstrated the key role of the synthesis temperature on the topology of fluorinated MOFs [26]. At high temperatures and in solvothermal conditions, dimethylformamide solvent (DMF) hydrolyses into dimethylammonium cation $[Hdma]^+$ and formate anion $(HCOO)^-$ [27,28]. The fragments produced by the DMF decomposition can either enter into the coordination sphere of the metal cation or act as a template. The network dimensionality can also be tuned by increasing the synthesis temperature, as demonstrated for hybrid fluorozincates prepared in acetonitrile (MeCN) [29].

Herein, we highlight the determining role of the solvent in the crystallization of zinc fluoro-aminotetrazolates. The solvothermal reaction of identical starting mixtures of $ZnF_2/HF_{aq}/H$*amtetraz* was explored in different solvents. Two new hybrid fluorides $(Zn_4F_4(amtetraz)_4)\cdot H_2O$ (1) and $(Zn_4F_4(H_2O)(amtetraz)_4)\cdot H_2O$ (2) were identified in methanol/water and water, respectively. Their structures are compared to the previously reported networks $[Hdma]\cdot(Zn_4F_5(amtetraz)_4)$ and $[NH_4]\cdot(Zn_4F_5(amtetraz)_4)\cdot 3H_2O$, respectively prepared in dimethylformamide and acetonitrile [24,29]. Lastly

* Corresponding author.
E-mail address: vincent.maisonneuve@univ-lemans.fr (V. Maisonneuve).

https://doi.org/10.1016/j.jfluchem.2017.12.005
Received 18 July 2017; Received in revised form 6 December 2017; Accepted 7 December 2017
Available online 09 December 2017
0022-1139/

Table 1
Selected inter-atomic distances of zincate groups in $(Zn_4F_4(amtetraz))\cdot H_2O$ (1) and $(Zn_4F_4(H_2O)(amtetraz)_4)\cdot H_2O$ (2).

	1			2		
	Zn-(F/N)	d, Å	Cluster, *Geometry*	Zn-(F/N/O)	d, Å	Cluster, *Geometry*
Layer B	Zn(1)-F(2)	1.981 (6)	ZnF_2N_3 *trigonal bipyramid*	Zn(1)-F(1)	1.979 (3)	ZnF_2N_3 *trigonal bipyramid*
	Zn(1)-F(1)	1.988 (6)		Zn(1)-F(2)	1.982 (3)	
	Zn(1)-N(6)	2.019 (8)		Zn(1)-N(6)	2.011 (4)	
	Zn(1)-N(12)	2.103 (7)		Zn(1)-N(21)	2.091 (4)	
	Zn(1)-N(15)	2.154 (8)		Zn(1)-N(18)	2.126 (4)	
	< Zn-F > = 1.985 Å < Zn-N > = 2.092 Å			< Zn-F > = 1.981 Å < Zn-N > = 2.076 Å		
	Zn(2)-F(2)	1.979 (5)	ZnF_2N_3 *trigonal bipyramid*	Zn(2)-F(2)	1.982 (3)	ZnF_2N_3O *octahedron*
	Zn(2)-F(1)	2.019 (5)		Zn(2)-F(1)	2.014 (3)	
	Zn(2)-N(1)	1.963 (9)		Zn(2)-N(1)	2.054 (4)	
	Zn(2)-N(14)	2.079 (8)		Zn(2)-N(17)	2.137 (4)	
	Zn(2)-N(11)	2.127 (7)		Zn(2)-N(20)	2.141 (4)	
				Zn(2)-OW(1)	2.363 (7)	
	< Zn-F > = 1.999 Å < Zn-N > = 2.056 Å			< Zn-F > = 1.998 Å < Zn-N > = 2.111 Å		
Layer A	Zn(3)-F(4)	2.033 (5)	ZnF_2N_4 *octahedron*	Zn(3)-F(4)	2.027 (3)	ZnF_2N_4 *octahedron*
	Zn(3)-F(3)	2.060 (5)		Zn(3)-F(3)	2.077 (3)	
	Zn(3)-N(17)	2.083 (8)		Zn(3)-N(15)	2.094 (4)	
	Zn(3)-N(20)	2.114 (8)		Zn(3)-N(11)	2.110 (4)	
	Zn(3)-N(9)	2.137 (8)		Zn(3)-N(4)	2.120 (4)	
	Zn(3)-N(3)	2.186 (8)		Zn(3)-N(8)	2.195 (4)	
	< Zn-F > = 2.046 Å < Zn-N > = 2.130 Å			< Zn-F > = 2.052 Å < Zn-N > = 2.130 Å		
	Zn(4)-F(4)	2.015 (5)	ZnF_2N_4 *octahedron*	Zn(4)-F(3)	2.019 (3)	ZnF_2N_4 *octahedron*
	Zn(4)-F(3)	2.021 (5)		Zn(4)-F(4)	2.049 (3)	
	Zn(4)-N(4)	2.114 (9)		Zn(4)-N(9)	2.116 (4)	
	Zn(4)-N(8)	2.156 (8)		Zn(4)-N(3)	2.147 (4)	
	Zn(4)-N(18)	2.183 (7)		Zn(4)-N(14)	2.203 (4)	
	Zn(4)-N(21)	2.234 (8)		Zn(4)-N(12)	2.252 (4)	
	< Zn-F > = 2.018 Å < Zn-N > = 2.172 Å			< Zn-F > = 2.034 Å < Zn-N > = 2.180 Å		

the photoluminescent properties of the compounds prepared in methanol (**2**), in DMF and MeCN were investigated, since coordination polymers based on Zn^{2+} and azole ligands have been reported as promising candidates for potential applications as photoactive materials: chemical sensors or light emitting diodes (LEDs) [30,31].

2. Results and discussion

2.1. Crystal structure description and comparison with other known structures

Compounds 1 and 2 crystallize in the orthorhombic and monoclinic systems, respectively; both phases show a 3D neutral framework in which disordered water molecules are inserted. 1 and 2, with non-centrosymmetric space groups, exhibit roughly similar structures that are confirmed by the examination of inter-atomic distances (Table 1), at the exception of one oxygen atom. The 3D frameworks can be described from two types of (001) layers connected along the *c* axis by anionic ligands *amtetraz*$^-$ in the connection mode N1,N2,N4 as defined in [24] (Fig. 1(a) and (b)).

The first type of layer (A), located at z = 0 and ½ for 1 and at z = 0 for 2, results from the association of $_\infty[ZnFN_4]$ chains by tetrazolate anions in N1,N2,N3,N4 bridging modes (Fig. 2(a)). The zinc atoms, Zn (3) and Zn(4), adopt an octahedral coordination and are surrounded by two fluorine atoms and four nitrogen atoms from independent organic anions. $Zn(3)F_2N_4$ and $Zn(4)F_2N_4$ entities, linked by fluorine corners with *trans* or *cis* orientation, respectively, alternate in these original chains. At z = ¼ and z = ¾ for 1 (B layer) and at z = ½ for **2** (B' layer), the second type of layers is observed, in which the tetrazolate linkers connect the chains of zinc polyhedra in N1,N2,N3,N4 bridging mode (Fig. 2(b)).

In 1, evidenced in a mixture of methanol and water, the ZnF_2N_3 (Zn (1) and Zn(2)) units share adjacent and opposite fluorine corners to form $_\infty[ZnFN_3]$ *cis-trans* chains. In **2**, obtained with water only, a similar condensation is observed but the metal cations adopt a trigonal bipyramidal geometry in $Zn(1)F_2N_3$ and an octahedral geometry in Zn(2) F_2N_3O. Therefore, in absence of methanol, water molecules complete the immediate coordination sphere of Zn(2) cations. If water molecules are mentally ignored in 1 and 2, both structures present a same architecture with a calculated porosity of 19% (PLATON software [32]). It must be noted that both structures 1 and 2 can also be described as inorganic chains connected by *amtetraz* anions along two other perpendicular directions. A similar construction is observed for two other compounds, $[NH_4]\cdot(Zn_4F_5(amtetraz)_4)\cdot 3H_2O$ and $[Hdma]\cdot(Zn_4F_5(amtetraz)_4)$, also prepared in identical reaction mixtures but in different solvents, respectively acetonitrile (MeCN) and dimethylformamide (DMF) (Fig. 3) [24,29].

In $[NH_4]\cdot(Zn_4F_5(amtetraz)_4)\cdot 3H_2O$ and $[Hdma]\cdot(Zn_4F_5(amtetraz)_4)$, two types of [100] chains are distinguished (Fig. 4). These chains, in which zinc cations adopt octahedral or trigonal bipyramidal coordinations, are linked by tetrazolate anions in the N1,N2,N4 bridging mode as observed in (1) and (2). The first *trans*-chain $_\infty[ZnFN_4]$ results from the connection of ZnF_2N_4 octahedra by two opposite F^- vertices while the second *trans*-chain $_\infty[Zn_2F_3N_4]$ results from the condensation of two ZnF_3N_2 polyhedra by one (F-F) edge, to give dimeric units that are further connected by opposite F^- corners. The difference between both structures is the relative orientation of chains (Fig. 3), governed by the symmetry elements ($P2_1/c$ for $[NH_4]\cdot(Zn_4F_5(amtetraz)_4)\cdot 3H_2O$ and $P2/m$ for $[Hdma]\cdot(Zn_4F_5(amtetraz)_4)$).

Interestingly, the formation of *trans*-chains linked by organic ligands in N1-N2-N4 bridging mode is formed in aprotic polar solvents (DMF, MeCN), whereas with protic polar solvents (methanol, water), both

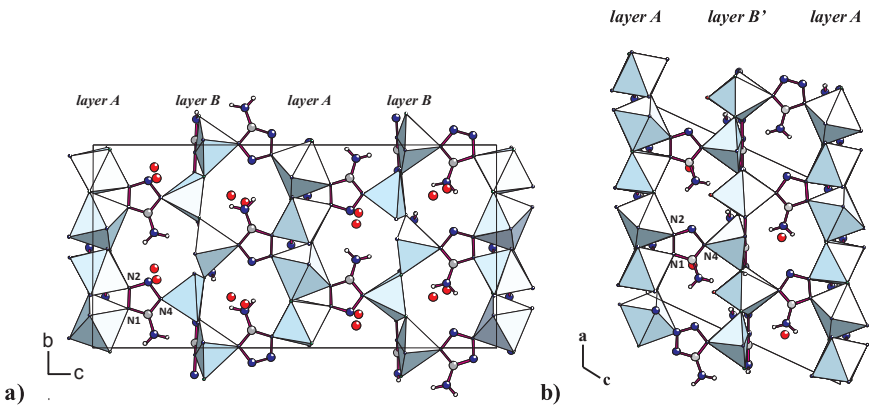

Fig. 1. (a) [100] projection of $(Zn_4F_4(amtetraz)_4)\cdot H_2O$ (1) built up from (A,B) layers. (b) [010] projection of $(Zn_4F_4(H_2O)(amtetraz)_4)\cdot H_2O$ (2) built up from (A,B') layers.

trans and *cis* chains are observed and both N1-N2-N4 and N1-N2-N3-N4 coordination modes of azole ligands are favoured (Table 2). To the best of our knowledge, there are no studies clarifying the effect of protic vs. aprotic solvents in the crystallization of MOFs. However we can suppose that the structural variety in the reported hybrid structures results from the difference in polarity and solvation effect in protic and aprotic solvents. In protic solvents, such as water and methanol, two coordination modes are observed due to presence of δ^+ hydrogen atoms, which can more effectively solvate the tetrazolate anion through hydrogen bonds. This higher stabilization of the anionic tetrazolate cycle allows the formation of both N1-N2-N4 and N1-N2-N3-N4 bridging modes and therefore *cis* and *trans* chains. In the case of aprotic solvents, no hydrogen bonds can be established and the tetrazolate anionic cycle is stabilized via van der Waals interactions, weaker than the hydrogen bonds observed in protic solvents. As a result, only N1,N2-N4 connection mode and chains with a *trans* geometry are observed.

2.2. Thermal behaviour of 1

The thermal behaviour of $(Zn_4F_4(amtetraz)_4)\cdot H_2O$ (1) was explored by thermogravimetric experiments and X-ray thermodiffraction (Fig. 5). The TGA curve shows three weight losses: dehydration occurs below 130 °C giving ZnF(*amtetraz*) (exp.: 2.8%, calc. 2.6%). The anhydrous phase is stable up to 320 °C. Then, from 320 °C to 400 °C, fluoride species and organic entities are eliminated and leave $Zn(CN)_2$ (exp.: 44.1%, calc. 44.4%). Finally the hydrolysis of zinc cyanide leads to the formation of zinc oxide (exp.: 5.9%, calc. 5.8%). X-ray thermodiffraction is in good agreement with TGA analysis. During the dehydration of $Zn_4F_4(amtetraz)_4)\cdot H_2O$, the framework is stable up to 300 °C. Above 300 °C, the structure collapses and ZnO is obtained as the final residue.

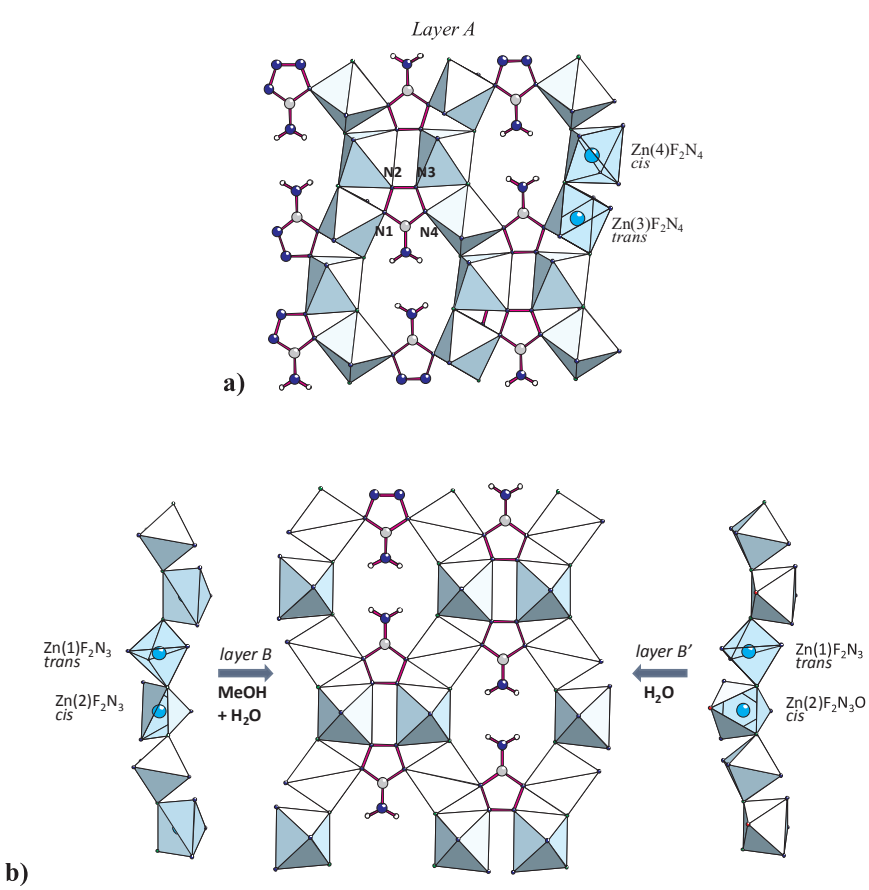

Fig. 2. (a) View of A layers found in $(Zn_4F_4(amtetraz)_4)\cdot H_2O$ (1) and $(Zn_4F_4(H_2O)(amtetraz)_4)\cdot H_2O$ (2). (b) View of B or B' layers, respectively found in $(Zn_4F_4(amtetraz)_4)\cdot H_2O$ (1) and $(Zn_4F_4(H_2O)(amtetraz)_4)\cdot H_2O$ (2).

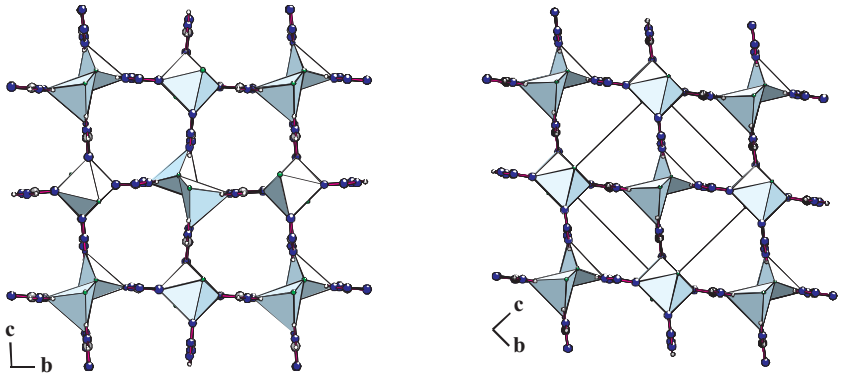

Fig. 3. [100] projection of $[NH_4]\cdot(Zn_4F_5(amtetraz)_4)\cdot 3H_2O$ (left) and $[Hdma]\cdot(Zn_4F_5(amtetraz)_4)$ (right). NH_4^+, H_2O or $Hdma^+$ entities in the cavities are omitted for clarity.

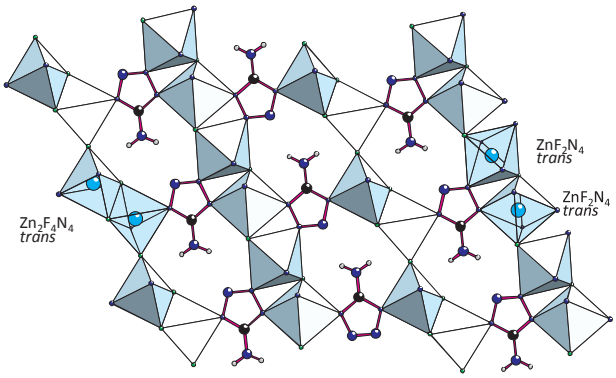

Fig. 4. View of the *trans-chains* observed in $[NH_4]\cdot(Zn_4F_5(amtetraz)_4)\cdot 3H_2O$ and $[Hdma]\cdot(Zn_4F_5(amtetraz)_4)$.

2.3. Luminescence properties

The origin of luminescence in MOFs is generally ascribed to the presence of organic ligands that often contain aromatic or π conjugated systems. In addition, metallic centres can also contribute to the luminescence properties, usually lanthanides or *d* block elements [33–35].

The photoluminescence spectroscopic characterization is reported for **1** as well as for $[NH_4]\cdot(Zn_4F_5(amtetraz)_4)$ and $[Hdma]\cdot(Zn_4F_5(amtetraz)_4)$). All samples were excited at 240 nm. Both $[NH_4]\cdot(Zn_4F_5(amtetraz)_4)$ and $[Hdma]\cdot(Zn_4F_5(amtetraz)_4)$) display ultraviolet emission, with a maximum peak respectively at 302 nm and 306 nm. $(Zn_4F_4(amtetraz)_4)\cdot H_2O$ shows a slightly red-shifted emission with a maximum at 330 nm (Fig. 6).

In all three cases, the broad band emissions can be ascribed to π–π* intra-ligand fluorescence transitions, as it has already been observed for triazole based frameworks [36]. The spectral variation can be explained by the difference of the bridging modes between aminotetrazolate ligands and the metallic centres. Indeed, the $amtetraz^-$ linker in $[NH_4]\cdot(Zn_4F_5(amtetraz)_4)$ and $[Hdma]\cdot(Zn_4F_5(amtetraz)_4)$ is in a N1-N2-N4 bridging mode in all directions while for $(Zn_4F_4(amtetraz)_4)\cdot H_2O$ (1) both N1-N2-N4 and N1-N2-N3-N4 modes can be observed. To fully understand the luminescent properties of these compounds, extended studies are needed and will be soon performed at other excitation wavelengths, in particular visible wavelengths excitation [37].

3. Conclusion

We report herein the synthesis and the structural characterisation of two new fluorinated zinc MOFs, $(Zn_4F_4(amtetraz)_4)\cdot H_2O$ (1) and $(Zn_4F_4(H_2O)(amtetraz)_4)\cdot H_2O$ (2). Both hybrid compounds were prepared from an identical reaction mixture but in different solvents, water and water/methanol mixture. The comparison of 1 and 2 with two other architectures prepared in acetonitrile and dimethylformamide, $[NH_4]\cdot(Zn_4F_5(amtetraz)_4)$ and $[Hdma]\cdot(Zn_4F_5(amtetraz)_4)$), demonstrates clearly that the crystallization of hybrid fluorozincates is strongly dependent on the nature of the solvent. In fact, not only zinc can display bipyramidal and octahedral geometries but also the organic ligand can establish N1-N2-N4 and N1-N2-N3-N4 bridging modes between the inorganic 1D chains. Owing to the remarkable luminescence properties of zinc compounds, the photoluminescent behaviour of these compounds was investigated; however for an excitation at 240 nm, none of the studied compounds show important luminescent response since the shift between excitation and emission is only of about 50 nm.

4. Experimental

4.1. Synthesis

Both hybrid fluorozincates were obtained from a reaction mixture $ZnF_2/HF_{aq}/Hamtetraz$ with the molar ratio 10/80/10 in 10 mL of solvent. The starting reactants were 78 mg of ZnF_2, 2.634 mL of 4% hydrofluoric acid solution (2.3 mol L^{-1}) prepared from 40% HF (22.8 mol L^{-1}), 78 mg of 5-aminotetrazole monohydrate '$Hamtetraz\cdot H_2O$' and 10 mL of solvent (methanol and/or H_2O). The mixture was heated in Teflon lined autoclaves in a CEM microwave oven at 160 °C during 1 h. For the synthesis of $(Zn_4F_4(amtetraz)_4)\cdot H_2O$ (1) 10 mL of water and methanol mixture in 1:1 ratio were used. When the solvent is water, parallelepipedic crystals of $(Zn_4F_4(H_2O)(amtetraz)_4)\cdot H_2O$ (2) are formed; however, it is worth to note that **2** crystallizes together with **1** systematically, despite all attempts to modify the synthesis conditions. The final products were washed with the solvent used during the synthesis, then filtered and dried at room

Table 2
Comparison between $(Zn_4F_4(amtetraz)_4)\cdot H_2O$ (1), $(Zn_4F_4(amtetraz)_4)\cdot H_2O$ (2), $[NH_4]\cdot(Zn_4F_5(amtetraz)_4)\cdot 3H_2O$ and $[Hdma]\cdot(Zn_4F_5(amtetraz)_4)$.

Compounds Solvent	chain 1		chain 2		Bridging mode of $amtetraz^-$
	Zn environment	*Coordination mode*	Zn environment	*Coordination mode*	
$(Zn_4F_4(amtetraz)_4)\cdot H_2O$ (1) *MeOH + H_2O*	ZnF_2N_4	*trans, cis*	ZnF_4N	*trans, cis*	N1,N2,N4 N1,N2,N3,N4
$(Zn_4F_4(H_2O)(amtetraz)_4)\cdot H_2O$ (2) *H_2O*	ZnF_2N_4	*trans, cis*	ZnF_4N + ZnF_4ON	*trans, cis*	N1,N2,N4 N1,N2,N3,N4
$[NH_4]\cdot(Zn_4F_5(amtetraz)_4)\cdot 3H_2O$ *MeCN*	ZnF_2N_4	*trans*	$Zn_2F_4N_4$	*trans*	N1,N2,N4
$[Hdma]\cdot(Zn_4F_5(amtetraz)_4)$ *DMF*	ZnF_2N_4	*trans*	$Zn_2F_4N_4$	*trans*	N1,N2,N4

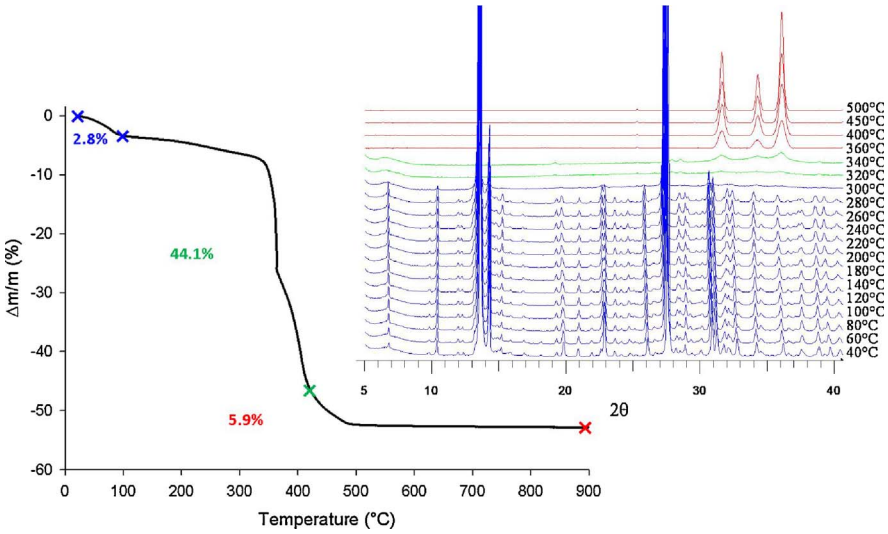

Fig. 5. Thermogravimetric curve and thermal evolution of the X-ray diffractograms of $(Zn_4F_4(amtetraz)_4)\cdot H_2O$ (1).

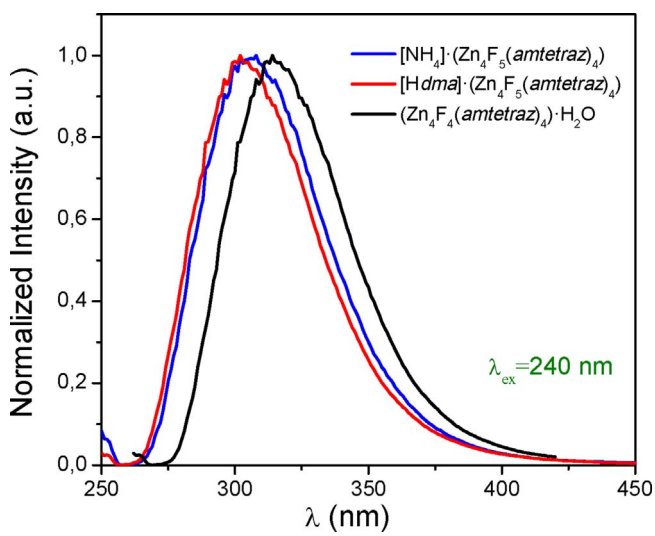

Fig. 6. Normalized emission spectra of hybrid fluorozincates prepared in different solvents (MeCN, DMF, MeOH) for an excitation at 240 nm.

temperature. Experimental and simulated XRD patterns of **1** and **2** can be found as Supplementary information (Figs. S1 and S2).

4.2. Single crystal X-ray structure determination

Crystals were selected and isolated under polarizing optical microscope and then mounted on MicroMount needles (MiTiGen) for single-crystal X-ray diffraction measurements. X-ray intensities were collected on a Bruker APEX II Quazar diffractometer (4 circle Kappa goniometer, CCD detector) using Iμs microfocus source (Mo-Kα radiation with λ = 0.71073 Å) at 296 K. The structure solutions were found by direct methods (TREF option) and extended by Fourier difference maps and subsequent refinements (SHELXL-2014 software [38]). The nature of atoms was differentiated from bond distance considerations. All non-hydrogen atoms were refined anisotropically and the hydrogen atoms of the amine group in $[amtetraz]^-$ ligand were geometrically constrained by HFIX 93 option. Oxygen atoms of hosted water molecules were statistically distributed on symmetry related atomic positions and they were refined isotropically. The hydrogen atoms of water molecules were not localized. The final reliability ratios converged to $R_1 = 0.0457/wR_2 = 0.956$ for 1 and $R_1 = 0.0374/wR_2 = 0.1068$ for **2**. Structure determination details are provided in Table 3. Atomic positions, anisotropic displacement parameters and selected interatomic distances are given in the Supplementary information (Tables S1-S5).

Table 3
Crystallographic data of $(Zn_4F_4(amtetraz)_4)\cdot H_2O$ (1) and $(Zn_4F_4(H_2O)(amtetraz)_4)\cdot H_2O$ (2).

	1	2
Empirical formula	$Zn_4F_4ON_{20}C_4H_{10}$	$Zn_4F_4O_2N_{20}C_4H_{12}$
M (g.mol^{-1})	691.8	709.8
Crystal system	orthorhombic	monoclinic
Space group	$Cmc2_1$	Cm
a (Å)	12.2953(8)	13.0404(3)
b (Å)	12.9607(7)	12.3343(3)
c (Å)	25.7891(16)	14.3326(4)
β (°)		116.857(1)
V (Å^3)	4109.6(4)	2056.6(1)
Z	8	4
ρ_{calc} (g cm^{-3})	2.236	2.292
μ(Mo, Kα) (mm^{-1})	4.696	4.698
F(000)	2704	1392
Unique reflections	3829	7779
Observed reflections [I > 2σ(I)]	3021	7498
Parameters	316	312
GOF on F^2	1.081	1.149
Final R indices [I > 2 σ(I)]	$R_1 = 0.0418$ $wR_2 = 0.0919$	$R_1 = 0.0374$ $wR_2 = 0.1068$
R indices (all data)	$R_1 = 0.0642$ $wR_2 = 0.1069$	$R_1 = 0.0388$ $wR_2 = 0.1078$
Largest diff. peak and hole (e/Å^3)	−0.570/0.739	−1.615/1.337
CCDC	1449121	1449120

Crystallographic data for the structures have been deposited to the Cambridge Crystallographic Data Center, with the following numbers: CCDC 1449121 for (Zn4F4(amtetraz)4)·H2O (1) and CCDC 1449120 for (Zn4F4(H2O)(amtetraz)4)·H2O (2). Copies of data can be obtained, free of charge, on application to the Director, CCDC, 12 Union Road, Cambridge CB2 1EZ, UK (fax: + 44 1223 336033 or e mail: deposit@ ccdc cam ac uk

4.3. Thermal characterization by TGA and X-ray thermodiffraction

Thermogravimetric analysis was carried out with a thermoanalyzer SETARAM TGA 92 under air flow with a heating rate of 3 °C/min from room temperature up to 900 °C. High temperature X-ray diffraction was performed under air flow in an Anton Parr XRK 900 high temperature furnace with a Panalytical X'Pert Pro diffractometer (CuK_α radiation). The sample was heated from 40 °C to 500 °C at a heating rate of 10 °C/min and measured at every 10 °C from room temperature to 400 °C and

every 50 °C from 400 °C to 500 °C. X-ray diffraction patterns were recorded in the 5–60° range with a scan time of 10 min.

4.4. Luminescence properties

Excitation and emission spectra were recorded with a SPEX Fluorolog FL212 spectrofluorometer. The excitation spectra were corrected for the variation of the incident flux and the emission spectra were corrected for the transmission of the monochromator and the response of the photomultiplier. All samples were excited at 240 nm.

Acknowledgements

The authors thank Le Mans Metropole and Conseil Départemental de la Sarthe (France) for funding V. Pimenta's PhD grant.

Appendix A. Supplementary data

Supplementary data associated with this article can be found, in the online version, at https://doi.org/10.1016/j.jfluchem.2017.12.005.

References

[1] L. Murray, M. Dincă, J.R. Long, Hydrogen storage in metal–organic frameworks, Chem. Soc. Rev. 38 (2009) 1294–1314.
[2] P. Horcajada, T. Chalati, C. Serre, B. Gillet, C. Sebrie, T. Baati, J.F. Eubank, D. Heurtaux, P. Clayette, C. Kreuz, J.-S. Chang, Y.K. Hwang, V. Marsaud, P.-N. Bories, L. Cynober, S. Gil, G. Férey, P. Couvreur, R. Gref, Porous metal–organic-framework nanoscale carriers as a potential platform for drug delivery and imaging, Nat. Mater. 9 (2010) 172–178.
[3] A.H. Chughtai, N. Ahmad, H.A. Younus, A. Laypkovand, F. Verpoort, Metal–organic frameworks: versatile heterogeneous catalysts for efficient catalytic organic transformations, Chem. Soc. Rev. 44 (2015) 6804–6849.
[4] J. Rocha, L.D. Carlos, F.A. Paz, D. Ananias, Luminescent multifunctional lanthanides-based metal–organic frameworks, Chem. Soc. Rev. 40 (2011) 926–940.
[5] T. Devic, C. Serre, High valence 3p and transition metal based MOFs, Chem. Soc. Rev. 43 (2014) 6097–6115.
[6] W. Ouellette, K. Darling, A. Prosvirin, K. Whitenack, K.R. Dunbar, J. Zubieta, Syntheses structural characterization and properties of transition metal complexes of 5,5′-(1,4-phenylene)bis(1H-tetrazole) (H_2bdt), 5′,5″-(1,1′-biphenyl)-4,4′-diylbis (1H-tetrazole) (H_2dbdt) and 5,5′,5″-(1,3,5-phenylene)tris(1H-tetrazole) (H_3btt), Dalton Trans. 40 (2011) 12288–12300.
[7] C.A. Black, J. Sánchez Costa, W.T. Fu, C. Massera, O. Roubeau, S.J. Teat, G. Aromí, P. Gamez, J. Reedijk, 3-D lanthanide metal-organic frameworks: structure, photoluminescence, and magnetism, Inorg. Chem. 48 (2009) 1062–1068.
[8] S.E. Russell, C. Gosset, X. Agache, C. Volkringer, N. Henry, R. Decadt, R. Van Deun, M. Visseaux, T. Loiseau, A new series of trivalent lanthanide (Ce, Pr, Nd, Sm, Eu, Gd, Tb, Dy) coordination polymers with a 1,2-cyclohexanedicarboxylate ligand: synthesis, crystal structure, luminescence and catalytic properties, CrystEngComm 18 (2016) 3594–3605.
[9] N. Ahmad, A.H. Chughtai, H.A. Younus, F. Verpoort, Discrete metal-carboxylate self-assembled cages: design, synthesis and applications, Coord. Chem. Rev. 280 (2014) 1–27.
[10] G. Aromi, L.A. Barrios, O. Roubeau, P. Gamez, Triazoles and tetrazoles: prime ligands to generate remarkable coordination materials, Coord. Chem. Rev. 255 (2011) 485–546.
[11] S.-Q. Bai, D.J. Young, T.S.A. Hor, Nitrogen-rich azoles as ligand spacers in coordination polymers, Chem. Asian J. 6 (2011) 292–304.
[12] Y. He, B. Li, M. O'Keeffe, B. Chen, Multifunctional metal–organic frameworks constructed from meta-benzenedicarboxylate units, Chem. Soc. Rev. 43 (2014) 5618–5656.
[13] W. Lu, Z. Wei, Z.-Y. Gu, T.-F. Liu, J. Park, J. Park, J. Tian, M. Zhang, Q. Zhang, T. Gentle, M. Boscha, H.-C. Zhou, Tuning the structure and function of metal–organic frameworks via linker design, Chem. Soc. Rev. 43 (2014) 5561–5593.
[14] D.-C. Zhong, X.-L. Feng, T.-B. Lu, Two organic–inorganic hybrid frameworks with unusual inorganic and organic connectivity, CrystEngComm 13 (2011) 2201–2203.
[15] D.J. Tranchemontagne, J.L. Mendoza-Cortés, M. O'Keeffe, O.M. Yaghi, Secondary building units, nets and bonding in the chemistry of metal–organic frameworks, Chem. Soc. Rev. 38 (2009) 1257–1283.
[16] Y.-B. Dong, Y.-Y. Jiang, J. Li, J.-P. Ma, F.-L. Liu, B. Tang, R.-Q. Huang, S.R. Batten, Temperature-dependent synthesis of metal–organic frameworks based on a flexible tetradentate ligand with bidirectional coordination donors, J. Am. Chem. Soc. 129 (2007) 4520–4521.
[17] D. Banerjee, J. Finkelstein, A. Smirnov, P.M. Forster, L.A. Borkowski, S.J. Teat, J.B. Parise, Synthesis and structural characterization of magnesium based coordination networks in different solvents, Cryst. Growth Des. 11 (2011) 2572–2579.
[18] D.-C. Zhong, W.-G. Lu, J.-H. Deng, Two three-dimensional cadmium(II) coordination polymers based on 5-amino-tetrazolate and 1,2,4,5-benzenetetracarboxylate: the pH value controlled syntheses, crystal structures and luminescent properties, CrystEngComm 16 (2014) 4633–4640.
[19] L. Li, S. Wang, T. Chen, Z. Sun, J. Luo, M. Hong, Solvent-dependent formation of Cd (II) coordination polymers based on a C2-Symmetric tricarboxylate linker, Cryst. Growth Des. 12 (2012) 4109–4115.
[20] H. Furukawa, K.E. Cordova, M. O'Keeffe, O.M. Yaghi, The chemistry and applications of metal-organic frameworks, Science 341 (2013) 1230444.
[21] D. Liu, G. Huang, C. Huang, X. Huang, J. Chen, X. You, Cadmium coordination polymers constructed from in situ generated amino-tetrazole ligand: effect of the conditions on the structures and topologies, Cryst. Growth Des. 9 (2009) 5117–5127.
[22] K. Darling, W. Ouellette, A. Prosvirin, S. Walter, K.R. Dunbar, J. Zubieta, Hydrothermal synthesis and structures of materials of the M(II)/tetrazole/sulfate family (M(II) = Co, Ni; Tetrazole = 3- and 4-pyridyltetrazole and pyrazinetetrazole), Polyhedron 58 (2013) 18–29.
[23] P. Pachfule, C. Dey, T. Panda, R. Banerjee, Synthesis and structural comparisons of five new fluorinated metal organic frameworks (F-MOFs), CrystEngComm 12 (2010) 1600–1609.
[24] V. Pimenta, J. Lhoste, A. Hemon-Ribaud, M. Leblanc, J.-M. Grenèche, L. Jouffret, A. Martel, G. Dujardin, V. Maisonneuve, Evidence of new fluorinated coordination compounds in the composition space diagram of FeF_3/ZnF_2–Hamtetraz-HF_{aq}. system, Cryst. Growth Des. 15 (2015) 4248–4255.
[25] M. Smida, J. Lhoste, V. Pimenta, A. Hemon-Ribaud, L. Jouffret, M. Leblanc, M. Dammak, J.-M. Grenèche, V. Maisonneuve, New series of hybrid fluoroferrates synthesized with triazoles: various dimensionalities and Mössbauer studies, Dalton Trans. 42 (2013) 15748–15755.
[26] V. Pimenta, Q.H.H. Le, L. Clark, J. Lhoste, A. Hémon-Ribaud, M. Leblanc, J.-M. Grenèche, G. Dujardin, P. Lightfoot, V. Maisonneuve, New iron tetrazolate frameworks: synthesis, temperature effect, thermal behaviour, Mössbauer and magnetic studies, Dalton Trans. 44 (2015) 7951–7959.
[27] T. Cottineau, M. Richard-Plouet, J.-Y. Mevellec, L. Brohan, Hydrolysis and complexation of N,N-dimethylformamide in new nanostructurated titanium oxide hybrid organic–inorganic sols and gel, J. Phys. Chem. C 115 (2011) 12269–12274.
[28] B.C. Challis, J.A. Challis, J. Zabicky (Ed.), The Chemistry of Amides, John Wiley & Sons, 1970.
[29] V. Pimenta, Q.H. Hanh Le, A. Hemon-Ribaud, M. Leblanc, V. Maisonneuve, J. Lhoste, Effect of the synthesis temperature on the dimensionality of hybrid fluorozincates, J. Fluorine Chem. 188 (2016) 164–170.
[30] X.-L. Qi, R.-B. Lin, Q. Chen, J.-B. Lin, J.-P. Zhang, X.-M. Chen, A flexible metal azolate framework with drastic luminescence response toward solvent vapors and carbon dioxide, Chem. Sci. 2 (2011) 2214–2218.
[31] C.-C. Shen, W.-T. Chen, R.-S. Liu, Zeolitic imidazolate framework $[Zn_2(IM)_4{\cdot}(DMF)]$ for UV-white light-emitting diodes, Dalton Trans. 41 (2012) 11885–11888.
[32] A.L. Spek, PLATON: A Multipurpose Crystallographic Tool, The Netherlands, Utrecht University, 2002.
[33] L.D. Carlos, R.A.S. Ferreira, V. de Zea Bermudez, B. Julián-López, P. Escribano, Progress on lanthanide-based organic–inorganic hybrid phosphors, Chem. Soc. Rev. 40 (2011) 536–549.
[34] L.-L. Zheng, H.- Xiang Li, J.-D. Leng, J. Wang, M.-L. Tong, Two photoluminescent metal–organic frameworks constructed from Cd3(μ3-OH) cluster or 1D Zn5(μ3-OH) 2(μ-OH)2 chain units and in situ formed bis(tetrazole)amine ligands, Eur. J. Inorg. Chem. (2008) 213–217.
[35] Y. Cui, Y. Yue, G. Qian, B. Chen, Luminescent functional metal-organic frameworks, Chem. Rev. 112 (2012) 1126–1162.
[36] H. Zhao, S.-Y. Zhou, C. Feng, N.-X. Wei, G.-G. Wang, Synthesis, characterization and luminescence of Cd(II) Zn(II) complexes with 1,2,3-triazole derivatives and in situ solvothermal decarboxylation of the ligands, Inorg. Chim. Acta 421 (2014) 169–175.
[37] K. Liu, H. Hu, J. Sun, Y. Zhang, J. Han, L. Wang, pH–value-controlled assembly of photoluminescent zinc coordination polymers in the mixed-ligand system, J. Mol. Struct. 1134 (2017) 174–179.
[38] G.M. Sheldrick, SHELXL-2014, Program for Crystal Structure Determination, Göttingen Univ., Germany, 2014.